Spatial symmetry modulation of planar Hall effect in Weyl semimetals

Yi-Wen Wei [1,2,3] Ji Feng,[4,5,6,*] and Hongming Weng [1,2,7,†]

[1]*Songshan Lake Materials Laboratory, Dongguan, Guangdong 523808, China*
[2]*Beijing National Laboratory for Condensed Matter Physics, Institute of Physics, Chinese Academy of Sciences, Beijing 100190, China*
[3]*School of Applied Science, Beijing Information Science and Technology University, Beijing 100192, China*
[4]*International Center for Quantum Materials, School of Physics, Peking University, Beijing 100871, China*
[5]*Collaborative Innovation Center of Quantum Matter, Beijing 100871, China*
[6]*CAS Center for Excellence in Topological Quantum Computation, University of Chinese Academy of Sciences, Beijing 100190, China*
[7]*School of Physical Sciences, University of Chinese Academy of Sciences, Beijing 100049, China*

The planar Hall effect in Weyl semimetals has been proposed as a key feature of chiral anomaly and nontrivial Berry curvature, while the effect of fundamental spatial symmetry remains to be explored. Here, we show with general symmetry analysis and lattice model calculations that the planar Hall effect can be significantly modulated by a certain class of spatial symmetry operations. The odd terms of conductivity with respect to magnetic field, including the linear terms, vanish in the plane perpendicular to the axis of twofold rotation (C_2) or the C_2 combined symmetry operations (mirror, twofold screw rotation, glide plane). When applying the magnetic field perpendicular to the glide plane, we find that the planar Hall conductivity in bulk forbidden by glide symmetry becomes nonzero in its quasi-two-dimensional counterpart with broken glide symmetry. It is further clarified that the nonzero planar Hall conductivity comes from surface states. This signature can be used to distinguish bulk and surface transport in Weyl semimetals.

I. INTRODUCTION

Weyl semimetals [1–11] host linear energy dispersions through the Weyl points in electronic band structure and exhibit remarkable chiral anomaly effect [12–14] of Weyl fermions. The chiral anomaly effect can induce a negative longitudinal resistance [14–19], under a magnetic field parallel to the electric field which is associated with the nontrivial Berry curvature in the semiclassical regime. Recently, the chiral anomaly has been proposed to give rise to a kind of transverse transport phenomenon in Weyl semimetals besides the negative longitudinal resistance [20–23], which is commonly called planar Hall effect (PHE) in subsequent studies [24–33]. By convention, the PHE [24,25,34–39] refers to the production of nonzero transverse voltage coplanar with the applied electric and magnetic fields. The transverse conductivity in PHE does not necessarily change its sign as that in the normal Hall effect when the magnetic field is reversed. It is not a true Hall response if the transverse conductivity is quadratic in magnetic field [28].

PHE does not solely originate from the chiral anomaly or the Berry curvature effect in Weyl semimetals. It can also be induced by the conventional anisotropic orbital magnetoresistance [40–43]. These two different origins of the PHE cannot always be clearly distinguished in experiments, because the experimentally observed quadratic magnetoresistance

supports both kinds of mechanisms [26,27,44–46]. It is worth noting that the Berry curvature could contribute to an additional linear magnetoresistance if the Weyl cone is tilted [23,24,47]. This linear magnetoresistance can thus be regarded as an indicator of the PHE induced by Berry curvature [33,45]. For the linear magnetoconductivity in Weyl semimetals, the previous theoretical analyses discussed the effects of band bending [48], band tilting [23,24,47,49–51], and the associated effect between spin-orbit coupling and momentum-dependent ferromagnetic exchange interaction [52]. Little attention has been paid to the role of spatial symmetry [53], which is a more fundamental and straightforward feature of crystals than band structures and usually brings strict constraints on the transport coefficients. Therefore, an aim of the present work is to investigate the influence of spatial symmetry on the emergence of linear magnetoconductivity in the PHE.

Another essential property of Weyl semimetals is the Fermi arc surface states [2,4,8]. However, it is challenging to separate the contribution of surface states from bulk states in transport [54–56]. In view of symmetry, the spatial symmetry of a plane in quasi-two-dimensional structure can be lower than that in bulk for nonsymmorphic lattices. The reduced symmetry in quasi-two-dimensional structure puts less constraints [56] on PHE, therefore probably brings different features compared with bulk. This inspires us that PHE could be used to separate surface transport from bulk. Therefore, a second aim of this work is to study the PHE in the quasi-two-dimensional structure and find a possible scenario to distinguish the bulk and surface transport. In this paper,

*jfeng11@pku.edu.cn
†hmweng@iphy.ac.cn

we studied the constraints of spatial symmetries on linear magnetoconductivity in PHE. Some spatial symmetry operations can reverse the sign of the magnetic-field components, thereby suppressing the appearance of linear magnetoconductivity. Specifically, the sign of the magnetic field can be flipped by twofold rotation (C_2) and C_2 combined operations; that is, mirror plane $C_2\mathcal{P}$, twofold screw rotation $\{C_2|t\}$, and the glide plane $\{C_2\mathcal{P}|t\}$, where $\mathcal{P}$ represents the spatial inversion and t is a fractional translation of a Bravais lattice vector. Our symmetry analyses showed that the linear terms of magnetoconductivity are absent in the plane perpendicular to the C_2 rotation axis, which is consistent with the linear magnetoconductivity observed in magnetic Weyl semimetal $Co_3Sn_2S_2$ [57]. The symmetry analyses were then verified by our numerical calculations based on a lattice model preserving glide symmetry but breaking time-reversal symmetry. Finally, if the glide symmetry in bulk is destroyed in its quasi-two-dimensional counterpart, the planar Hall conductivity forbidden by glide symmetry becomes nonzero. In this situation, the planar Hall conductivity is entirely contributed by the surface states. This signature can be used to characterize the transport of surface states in Weyl semimetals.

II. SPATIAL SYMMETRY ANALYSIS

In the framework of linear-response theory, the conductivity as a rank-2 tensor is related to the electric field E and the electron current J through the equation $J = \sigma E$. When an external magnetic field B is applied, the series expression of conductivity in the magnetic field can be categorized into odd and even order terms for the purpose of symmetry analysis. It is well known that the magnetic field is a pseudovector which is invariant under inversion. In point-group operations, C_2 and improper C_2 can change the sign of the magnetic field components, where the latter is equivalent to a reflection perpendicular to the rotation axis. Under C_2, the magnetic-field vector remains unchanged along the rotation axis and is reversed along the direction perpendicular to the rotation axis.

The planes vertical and parallel to C_2 axis are considered separately. In the plane vertical to the C_2 axis, J, E, and B all change signs and the equation $J_i = \sigma_{ij}(B)E_j$ becomes $-J_i = \sigma_{ij}(-B)(-E_j)$. i, j are the direction axes vertical to rotation axis. Therefore, it can be found that the odd-order terms of conductivity, including the linear part, are absent in the plane perpendicular to the (im)proper C_2 rotation axis. In this case, the second-order terms of the conductivity on the magnetic field may become dominant. In the plane parallel to the C_2 rotation axis, the linear terms of magnetoconductivity are allowed but still restricted by C_2 rotation. Under C_{2x} operation, $J_y = \sigma_{yx}(B_x, B_y)E_x$ becomes $-J_y = \sigma_{yx}(B_x, -B_y)E_x$, which guarantees that σ_{yx} only contains the odd order terms on B_y and $\sigma_{yx} = 0$ at $B_y = 0$. In essence, the zero σ_{yx} is protected by C_2 rotation after applying the magnetic field parallel to the rotation axis [44]. Once the C_{2x} related symmetry is destroyed by the surface in nonsymmorphic lattice [56], σ_{yx} is allowed to be nonzero.

The above spatial symmetry-based analyses are performed without any approximation, and thus apply in general. However, it should be noted that the time-reversal symmetry also restricts the microscopic dynamics of electrons, as revealed

TABLE I. Symmetry analysis of PHE when the C_2 rotation axis is vertical or parallel to the observed xy plane. All the symmetry-allowed linear terms of conductivity on the magnetic field B or magnetization M are listed below.

Axis	Conductivity	Linear terms $\propto$
C_{2z}	σ_{xx}, σ_{yx}	M_z
C_{2x}	σ_{xx}	B_x, M_x, B_xM_x
	σ_{yx}	B_y, B_yM_x

by the famous Onsager reciprocal relation [58,59] where $\sigma_{xx}(B) = \sigma_{xx}(-B)$ and $\sigma_{xy}(B) = \sigma_{yx}(-B)$. These constraints required by time-reversal symmetry always work, regardless of the direction of magnetic field and thus are naturally suitable for the PHE where the magnetic field is coplanar with the electric field and the Hall voltage.

For a nonmagnetic system with time-reversal symmetry, the Onsager reciprocal relation indicates that the longitudinal conductivity $\sigma_{xx}(B)$ contains only even powers of the magnetic field, whereas the Hall conductivity $\sigma_{yx}(B)$ allows both even and odd contributions from B in principle. For a magnetic system without time-reversal symmetry, the Onsager relation is destroyed and we only need to consider the restrictions of spatial symmetry. For instance, when the magnetization is not parallel to the z axis, the C_{2z} rotation or C_{2z} combined symmetry (mirror or glide plane perpendicular to z; screw axis along z direction) of the lattice is broken if the magnetization is considered. In this case, the odd terms of B are retained in both $\sigma_{xx}(B)$ and $\sigma_{yx}(B)$. The vertical or in-plane C_2 rotation allowed linear terms of conductivity are listed in Table I. These features can be easily verified in experiments by changing the direction of magnetic field and magnetization. On the basis of these analyses, we can conclude that the conductivity of the PHE has the following characteristics: (i) the odd terms of $\sigma_{xx}(B)$ exist only in a time-reversal breaking system that has no C_{2z} rotation or C_{2z} combined symmetry. (ii) The odd terms of $\sigma_{yx}(B)$ are allowed if there is no C_{2z} or C_{2z} combined symmetry, regardless of whether the time-reversal symmetry is broken.

To gain insight into the modulation of spatial symmetry on Berry curvature effect, we then review the semiclassical theory of the PHE for Weyl semimetals and present detailed symmetry-based considerations about the linear magnetoconductivity. The Berry curvature effect has been involved in the equations of motion for Bloch electrons [60] and then in the Boltzmann equation [22,24,47,61]. By the relaxation-time approximation and ignoring high-order contributions, the longitudinal and Hall conductivity under an electric field along the x axis $E = E\hat{x}$ and a magnetic field in xy plane $B = B\cos\theta\hat{x} + B\sin\theta\hat{y}$ are given by

$$\sigma_{xx} = \frac{e^2\tau}{(2\pi)^3}\int d^3k D\left(-\frac{\partial f_{eq}}{\partial \epsilon_k}\right)\left[v_k^x + \frac{e}{\hbar}B\cos\theta(v_k \cdot \Omega_k)\right]^2,$$

$$(1)$$

$$\sigma_{yx} = \frac{e^2\tau}{(2\pi)^3}\int d^3k D\left(-\frac{\partial f_{eq}}{\partial \epsilon_k}\right)\left[v_k^x + \frac{e}{\hbar}B\cos\theta(v_k \cdot \Omega_k)\right]$$

$$\times \left[v_k^y + \frac{e}{\hbar}B\sin\theta(v_k \cdot \Omega_k)\right] + \frac{e^2}{\hbar}\int d^3k \Omega_k^z f_{eq}, \quad (2)$$

TABLE II. Symmetry modulations of the magnetoconductivity with a glide (or mirror) plane in the xy plane or twofold rotation (or screw) axis along the z direction. Because the spatial orientations x and y are equivalent in view of symmetry, we only present the analytic results of the magnetic field in the xy and xz planes.

Magnetic field	Conductivity	Order	Dominant terms
$\boldsymbol{B} = B\cos\theta\hat{x} + B\sin\theta\hat{y}$	σ_{xx}	2	$\frac{e^2 B^2}{\hbar^2}\left(v_{\boldsymbol{k}}^y \Omega_{\boldsymbol{k}}^y \cos\theta - v_{\boldsymbol{k}}^x \Omega_{\boldsymbol{k}}^y \sin\theta + v_{\boldsymbol{k}}^z \Omega_{\boldsymbol{k}}^z \cos\theta\right)^2$
	σ_{yy}	2	$\frac{e^2 B^2}{\hbar^2}\left(v_{\boldsymbol{k}}^x \Omega_{\boldsymbol{k}}^x \sin\theta - v_{\boldsymbol{k}}^y \Omega_{\boldsymbol{k}}^x \cos\theta + v_{\boldsymbol{k}}^z \Omega_{\boldsymbol{k}}^z \sin\theta\right)^2$
	σ_{yx}	2	$\frac{e^2 B^2}{\hbar^2}\left(v_{\boldsymbol{k}}^y \Omega_{\boldsymbol{k}}^y \cos\theta - v_{\boldsymbol{k}}^x \Omega_{\boldsymbol{k}}^y \sin\theta + v_{\boldsymbol{k}}^z \Omega_{\boldsymbol{k}}^z \cos\theta\right)\left(v_{\boldsymbol{k}}^x \Omega_{\boldsymbol{k}}^x \sin\theta - v_{\boldsymbol{k}}^y \Omega_{\boldsymbol{k}}^x \cos\theta + v_{\boldsymbol{k}}^z \Omega_{\boldsymbol{k}}^z \sin\theta\right)$
$\boldsymbol{B} = B\cos\theta\hat{x} + B\sin\theta\hat{z}$	σ_{xx}	1	$-\frac{eB}{\hbar}\sin\theta\,\Omega_{\boldsymbol{k}}^z \left(v_{\boldsymbol{k}}^x\right)^2$
	σ_{zz}	1	$-\frac{eB}{\hbar}\sin\theta\,\Omega_{\boldsymbol{k}}^z \left(v_{\boldsymbol{k}}^z\right)^2 + \frac{2eB}{\hbar}\sin\theta\,v_{\boldsymbol{k}}^z(\boldsymbol{v}_{\boldsymbol{k}}\cdot\boldsymbol{\Omega}_{\boldsymbol{k}})$
	σ_{zx}	1	$-\frac{eB}{\hbar}\cos\theta\,\Omega_{\boldsymbol{k}}^x v_{\boldsymbol{k}}^x v_{\boldsymbol{k}}^z + \frac{eB}{\hbar}\cos\theta\,v_{\boldsymbol{k}}^z(\boldsymbol{v}_{\boldsymbol{k}}\cdot\boldsymbol{\Omega}_{\boldsymbol{k}})$

where $D = [1 + e/\hbar(\boldsymbol{B}\cdot\boldsymbol{\Omega}_{\boldsymbol{k}})]^{-1}$. $\boldsymbol{\Omega}_{\boldsymbol{k}}$ and $\boldsymbol{v}_{\boldsymbol{k}}$ are the Berry curvature and the group velocity at the wave vector $\boldsymbol{k}$, respectively. f_{eq} is the equilibrium Fermi-Dirac distribution function with the energy dispersion $\epsilon_{\boldsymbol{k}}$. τ is the relaxation time, and e is the positive electron charge. The last term in Eq. (2) is the intrinsic anomalous Hall conductivity in terms of Berry curvature and is independent of $\boldsymbol{B}$. To clarify the dependence of conductivity on the magnetic field, we use the second-order Taylor expansion of the phase factor with $D = 1 - e/\hbar(\boldsymbol{B}\cdot\boldsymbol{\Omega}_{\boldsymbol{k}}) + (e/\hbar)^2(\boldsymbol{B}\cdot\boldsymbol{\Omega}_{\boldsymbol{k}})^2$. The linear and quadratic terms in Eqs. (1) and (2), expanded in magnetic field, are subsequently obtained. In reciprocal space, the mirror and C_2 rotation operations can change the signs of momentum $\boldsymbol{k}$, group velocity $\boldsymbol{v}_{\boldsymbol{k}}$, and the Berry curvature $\boldsymbol{\Omega}_{\boldsymbol{k}}$ along certain directions. Therefore, it is possible to make the linear terms vanish from the perspective of Brillouin-zone integration. The glide plane and the twofold screw rotation are expected to have the same effect as the mirror and C_2 rotation, because the additional fractional translation operation does not influence the above discussions about $\boldsymbol{v}_{\boldsymbol{k}}$ and $\boldsymbol{\Omega}_{\boldsymbol{k}}$.

Detailed expressions of the aforementioned arguments are presented here. The mirror or glide plane with respect to the xy plane connects the momentum $\boldsymbol{k}$ to $\boldsymbol{k}'$, satisfying $k_{x(y)} = k'_{x(y)}$ and $k_z = -k'_z$. The components of the group velocity and the Berry curvature obey the relations $v_{\boldsymbol{k}'}^{x(y)} = v_{\boldsymbol{k}}^{x(y)}$, $v_{\boldsymbol{k}'}^z = -v_{\boldsymbol{k}}^z$, $\Omega_{\boldsymbol{k}'}^{x(y)} = -\Omega_{\boldsymbol{k}}^{x(y)}$, and $\Omega_{\boldsymbol{k}'}^z = \Omega_{\boldsymbol{k}}^z$. Similarly, C_2 or the twofold screw axis along the z direction leads to $v_{\boldsymbol{k}'}^{x(y)} = -v_{\boldsymbol{k}}^{x(y)}$, $v_{\boldsymbol{k}'}^z = v_{\boldsymbol{k}}^z$, $\Omega_{\boldsymbol{k}'}^{x(y)} = -\Omega_{\boldsymbol{k}}^{x(y)}$, and $\Omega_{\boldsymbol{k}'}^z = \Omega_{\boldsymbol{k}}^z$ with the momentum relations $k_{x(y)} = -k'_{x(y)}$ and $k_z = k'_z$. By applying these symmetry considerations to the Brillouin-zone integration of the conductivity in Eqs. (1) and (2), the leading terms of the magnetoconductivity for different planes are formally analyzed in Table II. When the mirror (or glide) is in the xy plane or the twofold rotation (or screw) axis lies along the z direction, the linear terms of the longitudinal and Hall conductivities vanish in the xy plane as required by our general symmetry analysis on the vertical C_2 axis. In the xz plane, some linear terms of conductivities survive. σ_{xx} and σ_{zz} are in proportion to B_z, and σ_{zx} is in proportion to B_x. The results are consistent with our general symmetry analysis and can be extended to other directions if the corresponding symmetry operations are present.

On the other hand, the time-reversal symmetry requires that $\Omega_{-\boldsymbol{k}} = -\Omega_{\boldsymbol{k}}$ and $v_{-\boldsymbol{k}} = -v_{\boldsymbol{k}}$, which counteracts all the linear terms of B in Eqs. (1) and (2). Therefore, to observe any significant linear magnetoconductivity induced by the chiral anomaly and Berry curvature effect, a time-reversal-breaking system with a suitable measured plane is needed. However, if the band structure, group velocity, and the Berry curvature are significantly affected by the external magnetic field, the semiclassical approach becomes inapplicable. It would become meaningless to only discuss the linear parts because the magnetoconductivity may be present beyond perturbation theory [53,62]. We now apply above analyses to the recently observed PHE in Co$_3$Sn$_2$S$_2$, wherein the linear magnetoconductivity is attributed to the chiral anomaly [57]. Co$_3$Sn$_2$S$_2$ [63,64] has a rhombohedral structure with the space group of R-3m (No. 166), and the magnetization is approximately parallel to the threefold rotation axis along the z direction. The linear magnetoconductivity was observed in the xy plane, which conforms to our symmetry-based analysis because there is no twofold rotation (screw) axis along the z direction or mirror (glide) on the xy plane. In fact, PHE has also been observed in a series of nonmagnetic systems (TaAs [46], GdPbBi [26,28], Na$_3$Bi [28], Cd$_3$As$_2$ [30,31], VAl$_3$ [29], WTe$_2$ [45], MoTe$_2$ [32,40], NiTe$_2$ [41], and ZrTe$_5$ [33,65]). However, the applied magnetic field in experiments is not always strictly lying in the expected plane, which brings a component of the magnetic field perpendicular to that plane. In this case, the symmetry constraints on Hall conductivity are broken down, and the antisymmetric part of the measured Hall conductivity can be nonzero owing to the normal Hall effect and the Berry curvature effect. Thus, to investigate the pure in-plane transport, one should be careful to reasonably remove the effect of misalignment and precisely control the direction of the magnetic and electric fields.

III. LATTICE MODEL CALCULATIONS

To numerically show the modulation of spatial symmetry on the PHE, we perform magnetoconductivity calculations for a Weyl semimetal based on a time-reversal-symmetry-breaking cubic lattice model with glide plane symmetry
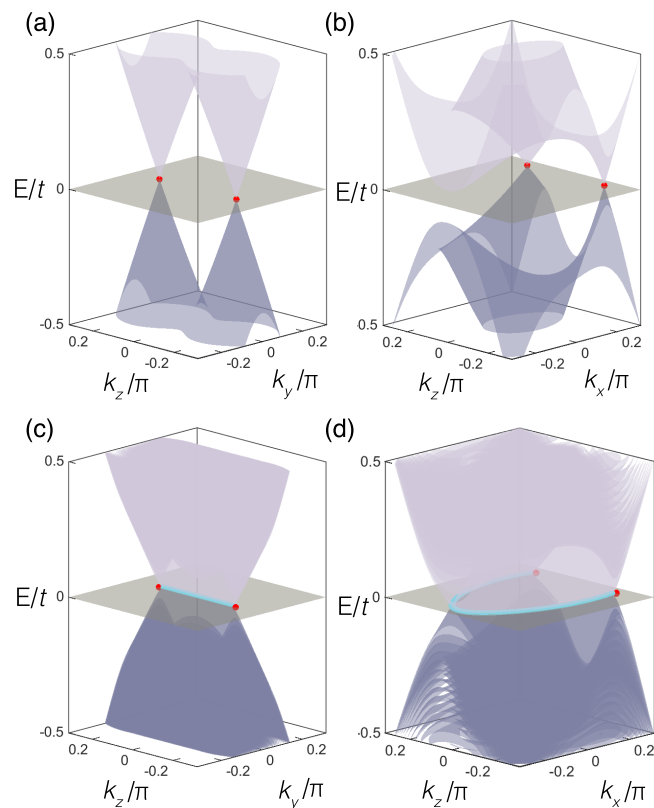
FIG. 1. The energy dispersion of the lattice model of the Weyl semimetal with glide symmetry, described by Eq. (3). Panels (a) and (b) show band structures with $k_x = 0.84$ and $k_y = 0$, respectively. Panels (c) and (d) show the band structures of the (100) and (010) slabs, respectively. A pair of Weyl nodes are marked by red dots, and the Fermi arcs are plotted in cyan.

[66,67]. The Hamiltonian is expressed as follows:

$$H_{\bm{k}} = (m - t\cos k_x - t\cos k_y - t\cos k_z)\sigma_0 s_3 + p\sigma_0 s_1$$

$$+ t\sin\frac{k_x - \phi}{2}\left(\cos\frac{k_x}{2}\sigma_1 s_1 + \sin\frac{k_x}{2}\sigma_2 s_1\right)$$

$$+ t\sin k_y\sigma_0 s_2 + t\sin k_z\sigma_3 s_1, \tag{3}$$

where the parameters $t = 0.1$ eV, $m = 2.5t$, $p = 0.6t$, and $\phi = 0.4$. σ and s describe the lattice and orbital degrees of freedom, respectively. σ_0 (s_0) is a 2×2-order identity matrix. σ_i and s_i ($i = 1, 2, 3$) are Pauli matrices. The band structures are shown in Figs. 1(a) and 1(b) with a pair of Weyl points located at $(0.84, 0, \pm 0.59)$, and the surface Fermi arc states are shown in Figs. 1(c) and 1(d) with (100) and (010) surfaces, respectively. The energy dispersions around the Weyl points in the k_x-k_z plane is slightly tilted. This feature is essential for linear magnetoconductivity according to previous studies [23,24,47]. The present lattice model holds the glide plane $\mathcal{G}$ consisting of a mirror in the xy plane and a half-translation along the x axis. The Hamiltonian under the glide plane $\mathcal{G}$ yields the relation

$$\mathcal{G}_{\bm{k}} H_{\bm{k}} \mathcal{G}_{\bm{k}}^{-1} = H_{\bm{k}'}, \tag{4}$$

where $\bm{k}' = (k_x, k_y, -k_z)$ and $\mathcal{G}_{\bm{k}} = e^{-ik_x/2}\sigma_1 s_0$. The related Berry curvature and group velocity satisfy $\bm{\Omega}_{\bm{k}'} = (-\Omega_{\bm{k}}^x, -\Omega_{\bm{k}}^y, \Omega_{\bm{k}}^z)$ and $\bm{v}_{\bm{k}'} = (v_{\bm{k}}^x, v_{\bm{k}}^y, -v_{\bm{k}}^z)$.
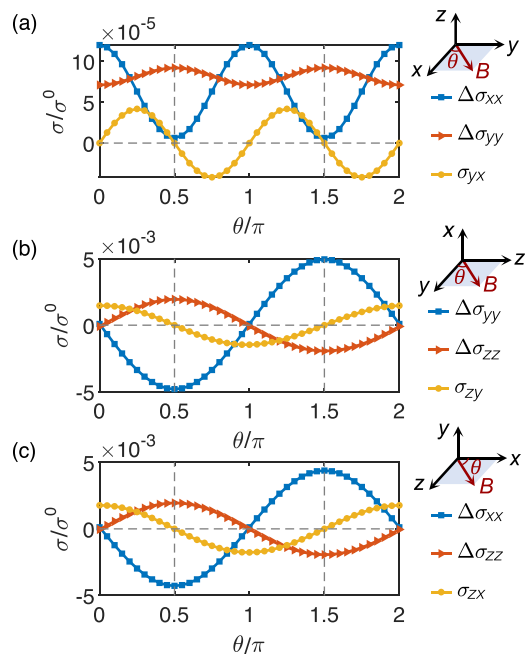
FIG. 2. The angular dependence of the longitudinal magnetoconductivity ($\Delta\sigma = \sigma - \sigma_{(B=0)}$) and Hall conductivities for the lattice model given by Eq. (3). In panels (a)–(c), the magnetic and electric fields are in the xy, yz, and xz planes, respectively, with $B = 4$ T. All conductivities are computed with the Fermi energy of $E_F = 0.02$ eV and are normalized by the longitudinal conductivity along the z direction without a magnetic field (σ^0). Note that the nonzero intrinsic anomalous Hall effect contribution σ_{zx} is ignored in panel (c), since it is independent of magnetic field.

The magnetoconductivities are computed based on this lattice model using Eqs. (1) and (2) with $T = 25$ K. The dependence of conductivity on the magnetic field $\bm{B}$ is discussed from two aspects: its direction and amplitude.

The longitudinal and Hall conductivity in xy, yz, and xz planes as functions of the angle θ between the magnetic and electric fields are calculated and plotted in Figs. 2(a)–2(c). When the magnetic field is in the xy plane, the in-plane magnetoconductivity shown in Fig. 2(a) displays sine or cosine oscillations with a period of π. The vanishing of linear terms meets the requirements of glide symmetry. Compared with the leading terms listed in Table II, the calculated σ_{xx} and σ_{yy} only display a $\cos 2\theta$ dependence without the $\sin 2\theta$ part, whereas the σ_{yx} only show $\sin 2\theta$ dependence without the $\cos 2\theta$ part. This is guaranteed by an additional symmetry composed of time reversal and a mirror in the yz plane. When the magnetic field is in the yz or xz plane, both the longitudinal conductivity and the Hall conductivity have a period of 2π, as shown in Figs. 2(b) and 2(c). This completely conforms to the symmetry requirements listed in Table II.

The magnetoconductivity as a function of B is shown in Fig. 3, where the angle θ is set to be zero (or $\pi/4$) in the longitudinal (or Hall) conductivity calculations as typical examples [24]. The magnetoconductivity σ_{yx}, σ_{yy}, and σ_{xx} quadratically depend on B, whereas σ_{zy}, σ_{zx}, and σ_{zz} show a linear dependence on B. According to the symmetry analysis in the last section, the glide plane in the xy plane eliminates all the linear
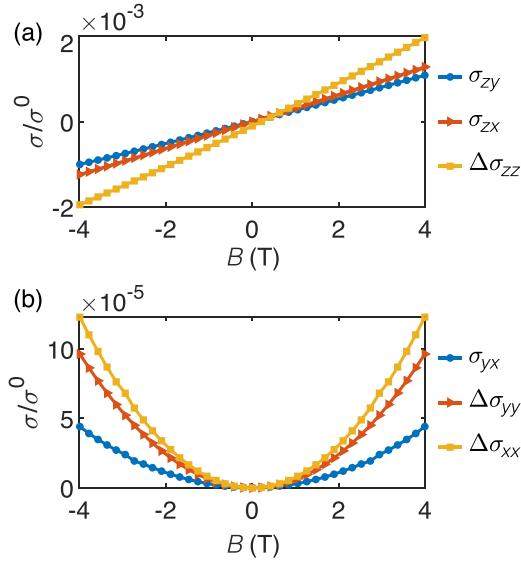
FIG. 3. The longitudinal conductivity ($\boldsymbol{B} \parallel \boldsymbol{E}$) and the Hall conductivity ($\theta = \pi/4$) as functions of the magnetic-field amplitude B for the lattice model given by Eq. (3). (a) The computed σ_{zy}, σ_{zx}, and σ_{yx} show a linear dependence on the magnetic field B. (b) σ_{yx}, σ_{yy}, and σ_{xx} show a quadratic dependence on B.

parts of the in-plane longitudinal and Hall magnetoconductivity. Therefore, we can see that the numerical results are in agreement with the symmetry analysis. These semiclassical numerical results quantitatively prove that the basic behavior of magnetoconductivity can be successfully predicted by our spatial symmetry analyses.

Having discussed the PHE in bulk, we now extend the discussion to quasi-two-dimensional transport which contains the contribution of surface states. It is obvious that the glide symmetry can be broken on the (100) slab by violating the fractional transnational symmetry along the x direction. The symmetry difference between the bulk and (100) slab remains after applying the external magnetic field parallel to the z direction. In this case, the magnetoconductivity in the (100) slab is expected to have a distinct behavior compared with the bulk transport [56]. In the bulk, the absence of σ_{zy}, shown in Fig. 2(b), is owing to the preserved glide plane. Under the glide plane operation, the electric current J_z changes sign and the electric field E_y remains unchanged, which forces σ_{zy} to be zero according to $J_z = \sigma_{zy}E_y$. However, in the (100) slab, the breaking of glide plane symmetry relaxes the constraint on σ_{zy}, and the resultant σ_{zy} is allowed to have nonzero values at $\theta = \pi/2$ and $3\pi/2$.

To prove our arguments and further explore the contribution of surface states, we study the planar Hall conductivity σ_{zy} in slabs with increasing layer thickness by employing Kubo-Streda formula [68–70], in which the interband transition could be properly taken into account. The magnetic field is handled by the standard Peierls substitution implemented with a magnetic supercell. The conductivities are evaluated with a finite electron lifetime broadening approximation to the Green's function [71]. Figure 4(a) shows the dependence of σ_{zy} on the number of layers n where the magnetic field is parallel to the z direction. When the slab is thicker than 10
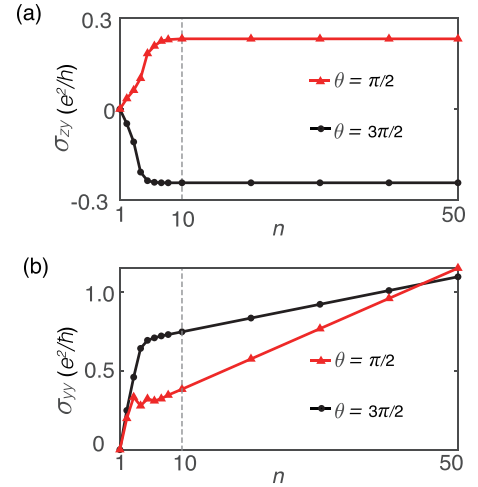
FIG. 4. The calculated in-plane magnetoconductivity in (100) slab. (a) The Hall conductivity σ_{zy} and (b) the longitudinal conductivity σ_{yy} as functions of the number of layers n. $\theta = \pi/2$ and $\theta = 3\pi/2$ represent the magnetic field along the z and $-z$ directions, respectively. A $1 \times 100 \times 1$ magnetic supercell is employed to implement the z-direction magnetic field during the magnetoconductivity calculations based on Kubo-Streda formula. The conductivities are evaluated with Green's functions broadened by a finite electron lifetime $\tau = 6.58 \times 10^{-14}$ s.

layers, σ_{zy} converges to a nonzero value, indicating that the bulk state does not contribute to the planar Hall conductivity. The longitudinal conductivity σ_{yy} is computed and plotted in Fig. 4(b) for comparison. σ_{yy} increases linearly with n after σ_{zy} has already converged. What is more, the increasing rate of σ_{yy} on thickness exactly matches the value of conductivity in bulk. Therefore, the linear increase of σ_{yy} originates from the increase of bulk states, and in turn the converged σ_{zy} should be attributed to surface contributions. In this way, glide symmetry breaking enables a pure surface transport.

IV. CONCLUSIONS

To summarize, we have demonstrated the influence of spatial symmetry in the PHE of Weyl semimetals. The symmetry analysis clearly shows that the odd terms of magnetoconductivity, including its linear part, vanish in the plane perpendicular to the rotation axis under C_2 or C_2 combined symmetry operations including mirror, twofold screw rotation, and glide plane. If the C_2 or C_2 combined symmetry is absent in a time-reversal-breaking system, a significant linear magnetoconductivity is allowed by the chiral anomaly and Berry curvature effect. It is then examined by our numerical results based on a lattice model preserving glide symmetry.

We further studied the magnetoconductivity in the quasi-two-dimensional slab, which contains the contribution of surface states. When the magnetic field is perpendicular to the glide plane, the planar Hall conductivity is found to be zero in bulk, whereas it is nonzero in the slab with broken glide symmetry. This distinct behavior between bulk and quasi-two-dimensional systems provides a signature to distinguish the

surface contributions to magnetoconductivity and paves a way to explore the surface Fermi arc states in Weyl semimetals.

[1] S. Murakami, New J. Phys. **9**, 356 (2007).

[2] X. Wan, A. M. Turner, A. Vishwanath, and S. Y. Savrasov, Phys. Rev. B **83**, 205101 (2011).

[3] A. A. Burkov and L. Balents, Phys. Rev. Lett. **107**, 127205 (2011).

[4] G. Xu, H. Weng, Z. Wang, X. Dai, and Z. Fang, Phys. Rev. Lett. **107**, 186806 (2011).

[5] G. B. Halász and L. Balents, Phys. Rev. B **85**, 035103 (2012).

[6] Z. Wang, Y. Sun, X.-Q. Chen, C. Franchini, G. Xu, H. Weng, X. Dai, and Z. Fang, Phys. Rev. B **85**, 195320 (2012).

[7] Z. Wang, H. Weng, Q. Wu, X. Dai, and Z. Fang, Phys. Rev. B **88**, 125427 (2013).

[8] S. Y. Xu, C. Liu, S. K. Kushwaha, R. Sankar, J. W. Krizan, I. Belopolski, M. Neupane, G. Bian, N. Alidoust, T. R. Chang, H. T. Jeng, C. Y. Huang, W. F. Tsai, H. Lin, P. P. Shibayev, F. C. Chou, R. J. Cava, and M. Z. Hasan, Science **347**, 294 (2015).

[9] H. Weng, C. Fang, Z. Fang, B. A. Bernevig, and X. Dai, Phys. Rev. X **5**, 011029 (2015).

[10] B. Q. Lv, H. M. Weng, B. B. Fu, X. P. Wang, H. Miao, J. Ma, P. Richard, X. C. Huang, L. X. Zhao, G. F. Chen, Z. Fang, X. Dai, T. Qian, and H. Ding, Phys. Rev. X **5**, 031013 (2015).

[11] S.-M. Huang, S.-Y. Xu, I. Belopolski, C.-C. Lee, G. Chang, B. Wang, N. Alidoust, G. Bian, M. Neupane, C. Zhang, S. Jia, A. Bansil, H. Lin, and M. Z. Hasan, Nat. Commun. **6**, 7373 (2015).

[12] S. L. Adler, Phys. Rev. **177**, 2426 (1969).

[13] J. S. Bell and R. Jackiw, Nuovo Cimento A **60**, 47 (1969).

[14] H. Nielsen and M. Ninomiya, Phys. Lett. B **130**, 389 (1983).

[15] D. T. Son and B. Z. Spivak, Phys. Rev. B **88**, 104412 (2013).

[16] A. A. Burkov, J. Phys.: Condens. Matter **27**, 113201 (2015).

[17] A. A. Burkov, Phys. Rev. B **91**, 245157 (2015).

[18] X. Huang, L. Zhao, Y. Long, P. Wang, D. Chen, Z. Yang, H. Liang, M. Xue, H. Weng, Z. Fang, X. Dai, and G. Chen, Phys. Rev. X **5**, 031023 (2015).

[19] C.-L. Zhang, S.-Y. Xu, I. Belopolski, Z. Yuan, Z. Lin, B. Tong, G. Bian, N. Alidoust, C.-C. Lee, S.-M. Huang, T.-R. Chang, G. Chang, C.-H. Hsu, H.-T. Jeng, M. Ne-upane, D. S. Sanchez, H. Zheng, J. Wang, H. Lin, C. Zhang, H.-Z. Lu, S.-Q. Shen, T. Neupert, M. Zahid Hasan, and S. Jia, Nat. Commun. **7**, 10735 (2016).

[20] Q. Li, D. E. Kharzeev, C. Zhang, Y. Huang, I. Pletikosić, A. Fedorov, R. Zhong, J. Schneeloch, G. Gu, and T. Valla, Nat. Phys. **12**, 550 (2016).

[21] Q. Li and D. E. Kharzeev, Nucl. Phys. A **956**, 107 (2016).

[22] S.-K. Yip, arXiv:1508.01010.

[23] V. A. Zyuzin, Phys. Rev. B **95**, 245128 (2017).

[24] S. Nandy, G. Sharma, A. Taraphder, and S. Tewari, Phys. Rev. Lett. **119**, 176804 (2017).

[25] A. A. Burkov, Phys. Rev. B **96**, 041110(R) (2017).

[26] N. Kumar, S. N. Guin, C. Felser, and C. Shekhar, Phys. Rev. B **98**, 041103(R) (2018).

[27] P. Li, C. H. Zhang, J. W. Zhang, Y. Wen, and X. X. Zhang, Phys. Rev. B **98**, 121108(R) (2018).

[28] S. Liang, J. Lin, S. Kushwaha, J. Xing, N. Ni, R. J. Cava, and N. P. Ong, Phys. Rev. X **8**, 031002 (2018).

[29] R. Singha, S. Roy, A. Pariari, B. Satpati, and P. Mandal, Phys. Rev. B **98**, 081103(R) (2018).

[30] M. Wu, G. Zheng, W. Chu, Y. Liu, W. Gao, H. Zhang, J. Lu, Y. Han, J. Zhou, W. Ning, and M. Tian, Phys. Rev. B **98**, 161110(R) (2018).

[31] H. Li, H.-W. Wang, H. He, J. Wang, and S.-Q. Shen, Phys. Rev. B **97**, 201110(R) (2018).

[32] F. C. Chen, X. Luo, J. Yan, Y. Sun, H. Y. Lv, W. J. Lu, C. Y. Xi, P. Tong, Z. G. Sheng, X. B. Zhu, W. H. Song, and Y. P. Sun, Phys. Rev. B **98**, 041114(R) (2018).

[33] J. Ge, D. Ma, Y. Liu, H. Wang, Y. Li, J. Luo, T. Luo, Y. Xing, J. Yan, D. Mandrus, H. Liu, X. C. Xie, and J. Wang, Natl. Sci. Rev. **7**, 1879 (2020).

[34] C. Goldberg and R. E. Davis, Phys. Rev. **94**, 1121 (1954).

[35] V. D. Ky, Phys. Status Solidi B **26**, 565 (1968).

[36] K. M. Seemann, F. Freimuth, H. Zhang, S. Blügel, Y. Mokrousov, D. E. Bürgler, and C. M. Schneider, Phys. Rev. Lett. **107**, 086603 (2011).

[37] A. A. Taskin, H. F. Legg, F. Yang, S. Sasaki, Y. Kanai, K. Matsumoto, A. Rosch, and Y. Ando, Nat. Commun. **8**, 1340 (2017).

[38] G. Yin, J.-X. Yu, Y. Liu, R. K. Lake, J. Zang, and K. L. Wang, Phys. Rev. Lett. **122**, 106602 (2019).

[39] N. Wadehra, R. Tomar, R. M. Varma, R. K. Gopal, Y. Singh, S. Dattagupta, and S. Chakraverty, Nat. Commun. **11**, 874 (2020).

[40] D. D. Liang, Y. J. Wang, W. L. Zhen, J. Yang, S. R. Weng, X. Yan, Y. Y. Han, W. Tong, W. K. Zhu, L. Pi, and C. J. Zhang, AIP Adv. **9**, 055015 (2019).

[41] Q. Liu, F. Fei, B. Chen, X. Bo, B. Wei, S. Zhang, M. Zhang, F. Xie, M. Naveed, X. Wan, F. Song, and B. Wang, Phys. Rev. B **99**, 155119 (2019).

[42] J. Yang, W. L. Zhen, D. D. Liang, Y. J. Wang, X. Yan, S. R. Weng, J. R. Wang, W. Tong, L. Pi, W. K. Zhu, and C. J. Zhang, Phys. Rev. Mater. **3**, 014201 (2019).

[43] J. Meng, H. Xue, M. Liu, W. Jiang, Z. Zhang, J. Ling, L. He, R. Dou, C. Xiong, and J. Nie, J. Phys.: Condens. Matter **32**, 015702 (2020).

[44] D. Rakhmilevich, F. Wang, W. Zhao, M. H. W. Chan, J. S. Moodera, C. Liu, and C.-Z. Chang, Phys. Rev. B **98**, 094404 (2018).

[45] P. Li, C. Zhang, Y. Wen, L. Cheng, G. Nichols, D. G. Cory, G.-X. Miao, and X.-X. Zhang, Phys. Rev. B **100**, 205128 (2019).

[46] Q. R. Zhang, B. Zeng, Y. C. Chiu, R. Schönemann, S. Memaran, W. Zheng, D. Rhodes, K.-W. Chen, T. Besara, R. Sankar, F. Chou, G. T. McCandless, J. Y. Chan, N. Alidoust, S.-Y. Xu, I. Belopolski, M. Z. Hasan, F. F. Balakirev, and L. Balicas, Phys. Rev. B **100**, 115138 (2019).

[47] D. Ma, H. Jiang, H. Liu, and X. C. Xie, Phys. Rev. B **99**, 115121 (2019).

[48] A. Cortijo, Phys. Rev. B **94**, 241105(R) (2016).

[49] Y.-W. Wei, C.-K. Li, J. Qi, and J. Feng, Phys. Rev. B **97**, 205131 (2018).

[50] K. Das and A. Agarwal, Phys. Rev. B **99**, 085405 (2019).

[51] A. Kundu, Z. B. Siu, H. Yang, and M. B. A. Jalil, New J. Phys. **22**, 083081 (2020).

[52] V. A. Zyuzin, Phys. Rev. B **104**, L140407 (2021).

[53] H. Tan, Y. Liu, and B. Yan, Phys. Rev. B **103**, 214438 (2021).

[54] A. C. Potter, I. Kimchi, and A. Vishwanath, Nat. Commun. **5**, 5161 (2014).

[55] P. Baireuther, J. A. Hutasoit, J. Tworzydło, and C. W. J. Beenakker, New J. Phys. **18**, 045009 (2016).

[56] G. Chang, J.-X. Yin, T. Neupert, D. S. Sanchez, I. Belopolski, S. S. Zhang, T. A. Cochran, Z. Chéng, M.-C. Hsu, S.-M. Huang, B. Lian, S.-Y. Xu, H. Lin, and M. Z. Hasan, Phys. Rev. Lett. **124**, 166404 (2020).

[57] B. Jiang, L. Wang, R. Bi, J. Fan, J. Zhao, D. Yu, Z. Li, and X. Wu, Phys. Rev. Lett. **126**, 236601 (2021).

[58] L. Onsager, Phys. Rev. **37**, 405 (1931).

[59] L. Onsager, Phys. Rev. **38**, 2265 (1931).

[60] D. Xiao, M.-C. Chang, and Q. Niu, Rev. Mod. Phys. **82**, 1959 (2010).

[61] K.-S. Kim, H.-J. Kim, and M. Sasaki, Phys. Rev. B **89**, 195137 (2014).

[62] Y. Choi, J. W. Villanova, and K. Park, Phys. Rev. B **101**, 035105 (2020).

[63] E. Liu *et al.*, Nat. Phys. **14**, 1125 (2018).

[64] Q. Wang, Y. Xu, R. Lou, Z. Liu, M. Li, Y. Huang, D. Shen, H. Weng, S. Wang, and H. Lei, Nat. Commun. **9**, 3681 (2018).

[65] T. Liang, J. Lin, Q. Gibson, S. Kushwaha, M. Liu, W. Wang, H. Xiong, J. A. Sobota, M. Hashimoto, P. S. Kirchmann, Z. X. Shen, R. J. Cava, and N. P. Ong, Nat. Phys. **14**, 451 (2018).

[66] H. Kim and S. Murakami, Phys. Rev. B **93**, 195138 (2016).

[67] C. Fang and L. Fu, Phys. Rev. B **91**, 161105(R) (2015).

[68] P. Streda, J. Phys. C: Solid State Phys. **15**, L717 (1982).

[69] L. Smrcka and P. Streda, J. Phys. C: Solid State Phys. **10**, 2153 (1977).

[70] N. A. Sinitsyn, J. E. Hill, H. Min, J. Sinova, and A. H. MacDonald, Phys. Rev. Lett. **97**, 106804 (2006).

[71] N. Nagaosa, J. Sinova, S. Onoda, A. H. MacDonald, and N. P. Ong, Rev. Mod. Phys. **82**, 1539 (2010).